Journal of Applied Electrochemistry **31**: 605–616, 2001.

Modelling of through-hole electrodeposition Part I: Effect of electrical migration

S.H. CHAN[1,2] and H.Y. CHEH[1,3]
[1]*Department of Chemical Engineering and Applied Chemistry, Columbia University, New York, NY 10027, USA*
[2]*Present address: Bristol–Myers Squibb Pharmaceutical Research Institute, New Brunswick, NJ 08903, USA*
[3]*Present address: Duracell, Berkshire Corporate Park, Bethel, CT 06801, USA*

Received 1 January 1999; accepted in revised form 21 November 2000

Key words: current distribution, polarization, surface concentration, through-hole electrodeposition

Abstract

A quantitative investigation was conducted on the effect of electrical migration on the current distribution in through-hole electrodeposition. Polarization, surface concentration and current distribution were computed as functions of the geometry of the through-hole, electrolyte flow rate, applied current density and concentration of the supporting electrolyte. Results were compared with those from a simplified model in which the electric field was neglected within the diffusion layer.

List of symbols

A_r	through-hole aspect ratio, $L_2/(2R_0)$
c_1	concentration of cupric ion (mol cm^{-3})
c_2, c_{H^+}	concentration of hydronium ion (mol cm^{-3})
$c_3, c_{SO_4^{2-}}$	concentration of sulfate ion (mol cm^{-3})
$c_4, c_{HSO_4^-}$	concentration of bisulfate ion (mol cm^{-3})
$c_{i\infty}$	bulk concentration of species i (mol cm^{-3})
$c_{H_2SO_4}$	concentration of sulfuric acid (mol cm^{-3})
c_{CuSO_4}	concentration of copper sulfate (mol cm^{-3})
D_1, D_2, D_3, D_4	diffusion coefficient of cupric ion, hydronium ion, sulfate ion and bisulfate ion (cm^2 s^{-1}), respectively
D_t, D_b, D_r, D_l	local diffusive flux through the control volume top face, bottom face, right face and left face (dimensionless)
E_r	equilibrium potential of electrode reaction (V)
F	faradaic constant (96 487 C equiv.$^{-1}$)
F_r, F_l	local convective flux through the control volume right face and left face (dimensionless)
i	local current density (A cm^{-2})
i_{avg}	average current density (A cm^{-2})
i_0	exchange current density (A cm^{-2})
$\bar{i}$	dimensionless local current density, $iR_0F/R_gT\kappa_\infty$
i/i_{avg}	normalized local current density
J_r, J_l, J_t, J_b	integrated total flux over the control volume right face, left face, top face and bottom face (dimensionless)
n	number of electrons transferred
Pe	Peclet number ($2\langle v_x\rangle R_0/D_1$)
P_r, P_l	local Peclet number on the control volume right face and left face
R_g	universal gas constant (8.314 J mol^{-1} K^{-1})
R_0	radius of the through-hole (cm)
r	ratio of the normality of the added ion to that of the counterion
T	temperature (K)
V_{app}	applied potential (V)
$\langle v_x\rangle$	average axial velocity (cm s^{-1})
v_x	axial velocity (cm s^{-1})
$\bar{v}_x$	dimensionless axial velocity
y	radial direction (cm)
z_1	charge of metal ion
z_2	charge of hydronium ion
z_3	charge of sulfate ion
z_4	charge of bisulfate ion

Greek letters

α_a, α_c	anodic and cathodic transfer coefficients
γ	order of the reaction
ζ	dimensionless axial distance, x/L_2
ζ_1	dimensionless axial distance, L_1/L_2
ζ_2	dimensionless axial distance, $xD_1/(2\langle v_x\rangle R_0^2)$
η_c	concentration overpotential (V)

η_s	surface overpotential (V)
θ_i	dimensionless concentration of species i
θ_i^0	guess value for the dimensionless concentration of species i
$\Delta\theta_i$	difference between the actual value and the guess value for the concentration
κ_∞	conductivity of the solution ($\Omega^{-1}\,cm^{-1}$)
ξ	dimensionless radial distance, y/R_0
ϕ	solution potential (V)
$\bar{\phi}$	dimensionless solution potential
ϕ_0	ohmic loss in the electrolyte (V)
$\bar{\phi}^0$	guess value for the dimensionless potential
$\Delta\bar{\phi}$	difference between the actual value and the guess value for the dimensionless potential

1. Introduction

Copper electrodeposition is one of the most important steps in the production of the multilayer printed wiring boards (MLB). Through-hole electrodeposition in MLB has been studied by many researchers over recent decades. As the technology of MLB advances, there is a continual increase of circuit densities on the boards. Also, the aspect ratio (length to diameter) of these through-holes has become higher and is expected to reach 20 during the next decade [1]. In practical applications, the uniformity of the copper distribution within a through-hole is a most important issue.

Most through-hole electrodeposition models have been based on a bulk-diffusion approach which separates the electrolyte into a thin diffusion layer region and a bulk region [1–5]. The variation of the depositing ion concentration is confined in a region close to the electrode surface. A uniform, bulk concentration is assumed at a finite distance away from the cathode. This result, known as the bulk-diffusion model, is good for electrolyte flow at a high velocity and for the concentration of the depositing ion to be low as compared to that of a supporting electrolyte. Because of the nonlinear nature of the Hagen–Poiseuille flow, the velocity profile is also linearized around the electrode surface by considering only the linear terms and neglecting all higher order terms. This model is widely used in the electrochemical literature because of its simplicity and its relatively short computational time.

Hazelbeck and Talbot [6] have included the effect of ionic migration in their analysis without separating the electrolyte into two regions. The Tafel equation was used to describe the kinetics of metal deposition. The solution was obtained by using the technique of orthogonal collocation with the dependent variables approximated by Legenedre polynomials. In their model, the metal ion concentration at the entrance region of the electrode was set to the bulk value, which is a generally a good assumption at high Peclet numbers.

More recently, Dudek and Fedkiw [7] and Goldbach et al. [8] modelled the electrodeposition of copper on a rotating disc electrode and a parallel plate reactor, respectively. Both included the effects of diffusion, migration and convection in their model. It was assumed that the metal deposition process occurs at steady state and is governed by the complete Butler–Volmer equation. In the former, the system of nonlinear equation was solved numerically using the finite element code while, in the later, it was solved using the control volume approach.

In the present investigation, a more rigorous model is developed for through-hole electrodeposition that considers the effect of ionic migration, the exact Hagen–Poiseuille profile, and the complete Butler–Volmer kinetic equation. We term this the 'field model'. The set of highly nonlinear partial differential equations is discretized using the control volume approach and solved numerically using an algebraic solver.

Results from both models are presented to demonstrate the importance of the effect of ionic migration on the current distribution and surface concentration. The importance of the field model was shown by using a system with low copper concentration (0.3 M $CuSO_4$ and 2.0 M H_2SO_4) as the base case for comparison. Results show that in cases where the amount of a supporting electrolyte is not in excess, the more rigorous field model should be used to predict the current profile.

2. Theoretical

2.1. *Bulk-diffusion model*

A through-hole model is shown schematically in Figure 1. Two counter electrodes are placed at a distance R_0 from the two ends of a working electrode. A steady-state, fully developed, laminar flow is assumed to occur as the electrolyte traverses from the left to the right. The velocity distribution is, therefore,

$$v_x = v_{max}\left[1 - \left(\frac{y}{R_0}\right)^2\right] \tag{1}$$

where v_x is the axial velocity, v_{max} is the maximum axial velocity, y is the radial coordinate from the centre of the through-hole, and R_0 is the radius of the through-hole.

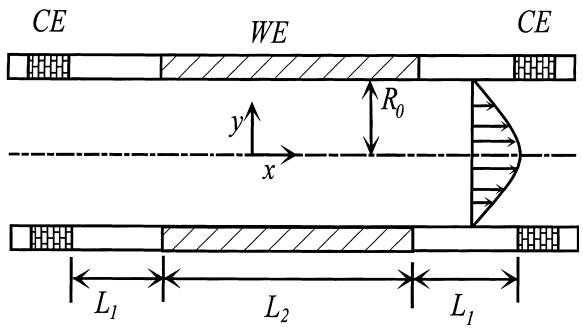

Fig. 1. Schematic diagram of the through-hole model.

Between the working and the counter electrode, an applied potential, V_{app}, is consumed by the ohmic loss in the electrolyte, ϕ_0, the concentration overpotential near the working electrode, η_c, the surface overpotential at the working electrode, η_s, and the equilibrium cell potential of the electrode reaction, E_r:

$$V_{app} = \phi_0 + \eta_c + \eta_s + E_r \tag{2}$$

The concentration overpotential is dependent on the surface concentration of the reacting species at the working electrode:

$$\eta_c = \frac{R_g T}{nF} \ln\left(\frac{c_{1s}}{c_{1\infty}}\right) \tag{3}$$

where R_g is the universal gas constant, T the temperature, n the number of electrons transferred in the electrochemical reaction, F is the faradaic constant, c_{1s} and $c_{1\infty}$ are the surface and bulk concentrations of the depositing ion, respectively.

At the surface of the electrode, the local reaction rate is given by the Butler–Volmer equation. That is,

$$i = i_0\left(\frac{c_{1s}}{c_{1\infty}}\right)^{\gamma}\left(\exp\left[\frac{\alpha_a nF}{R_g T}\eta_s(x)\right] - \exp\left[\frac{-\alpha_c nF}{R_g T}\eta_s(x)\right]\right) \tag{4}$$

where i_0 is the exchange current density at the reactant bulk concentration, α_a and α_c are the anodic and cathodic transfer coefficients, and x is the axial coordinate. The order of the reaction, γ [9], is given by

$$\gamma = \frac{2 - n\alpha_c}{2} \tag{5}$$

In the thin diffusion layer, the reactant concentration is governed by the convective diffusion equation. That is,

$$v_x \frac{\partial c_1}{\partial x} = D_1\left(\frac{1}{y}\frac{\partial}{\partial y}\left[y\frac{\partial c_1}{\partial y}\right] + \frac{\partial}{\partial x}\left[\frac{\partial c_1}{\partial x}\right]\right) \tag{6}$$

subject to the following boundary conditions:
At $y = 0$, for all x,

$$\frac{\partial c_1}{\partial y} = 0 \tag{7}$$

At $y = R_0$, for $-L_1 \le x \le 0$ and $L_2 \le x \le L_1 + L_2$,

$$\frac{\partial c_1}{\partial y} = 0 \tag{8}$$

At $y = R_0$, for $0 \le x \le L_2$,

$$D_1 \frac{\partial c_1}{\partial y} = \frac{i(x)}{nF} \tag{9}$$

At $x \le -L_1$, for all y,

$$c_1 = c_{1\infty} \tag{10}$$

At $x \ge 2L_1 + L_2$, for all y,

$$\frac{\partial c_1}{\partial x} = 0 \tag{11}$$

Previous authors [1–5] used a different form of boundary condition (10) by assuming that the concentration at the inlet of the working electrode ($x \le 0$) is equal to the bulk value. Generally, this assumption is good for very large Peclet numbers where the axial convective transport to the electrode surface is much greater than the axial diffusion term. The present boundary condition takes in account any back diffusion even in situations where the Peclet number is low.

In the bulk region where no concentration gradient is assumed to exist, the potential variation is governed by the Laplace equation. Thus,

$$\frac{1}{y}\frac{\partial}{\partial y}\left(y\frac{\partial \phi}{\partial y}\right) + \frac{\partial}{\partial x}\left(\frac{\partial \phi}{\partial x}\right) = 0 \tag{12}$$

subject to the following boundary conditions:
At $y = 0$, for all x,

$$\frac{\partial \phi}{\partial y} = 0 \tag{13}$$

At $y = R_0$, for $-L_1 \le x < 0$ and $L_2 \le x \le L_1 + L_2$,

$$\frac{\partial \phi}{\partial y} = 0 \tag{14}$$

At $y = R_0$, for $0 \le x \le L_2$,

$$\kappa_\infty \frac{\partial \phi}{\partial y} = i \tag{15}$$

At $x = 0$ and $x = L_2$, for all y,

$$\phi = 0 \tag{16}$$

where κ_∞ is the conductivity of the bulk solution.

In terms of the following dimensionless variables,

$$Pe = \frac{v_{max} R_0}{D_1} \quad A_r = \frac{L}{2R_0}, \quad \theta_1 = \frac{c_1}{c_{1\infty}} \tag{17}$$

$$\zeta_1 = \frac{L_1}{L_2}, \quad \bar{i}_2 = \frac{iR_0 F}{R_g T \kappa_\infty}, \quad \xi = \frac{y}{R_0} \tag{18}$$

$$\zeta = \frac{x}{L_2}, \quad \bar{v}_x = \frac{v_x}{v_{max}}, \quad \bar{i}_1 = \frac{iR_0}{nFD_1 c_{1\infty}} \tag{19}$$

the convective diffusion equation and boundary conditions are as follows:

$$\bar{v}_x \frac{\partial \theta_1}{\partial \zeta} = \frac{1}{Pe}\left(2Ar \frac{1}{\xi}\frac{\partial}{\partial \xi}\left[\xi \frac{\partial \theta_1}{\partial \xi}\right] + \frac{1}{2A_r}\frac{\partial}{\partial \zeta}\left[\frac{\partial \theta_1}{\partial \zeta}\right]\right) \quad (20)$$

At $\xi = 0$, for all ζ,

$$\frac{\partial \theta_1}{\partial \xi} = 0 \quad (21)$$

At $\xi = 1$, for $-\zeta_1 \le \zeta < 0$ and $1 \le \zeta \le 1 + \zeta_1$,

$$\frac{\partial \theta_1}{\partial \xi} = 0 \quad (22)$$

At $\xi = 1$, for $0 \le \zeta \le 1$,

$$\bar{i}_1 = \frac{\partial \theta_1}{\partial \xi} \quad (23)$$

At $\zeta \le -\zeta_1$, for all ξ,

$$\theta_1 = 1 \quad (24)$$

At $\zeta \ge 1 + \zeta_1$, for all ξ,

$$\frac{\partial \theta_1}{\partial \zeta} = 0 \quad (25)$$

Two important dimensionless variables are the Peclet number, Pe, and the aspect ratio, A_r. The Peclet number is a measure of the relative importance of the convective flux to the diffusive flux while the aspect ratio is defined as ratio of the length to the diameter of the through-hole.

Similarly, the dimensionless Laplace equation and boundary conditions are,

$$\frac{1}{\xi}\frac{\partial}{\partial \xi}\left[\xi \frac{\partial \bar{\phi}}{\partial \xi}\right] + \frac{1}{4A_r^2}\frac{\partial}{\partial \zeta}\left[\frac{\partial \bar{\phi}}{\partial \zeta}\right] = 0 \quad (26)$$

At $\xi = 0$, for all ζ,

$$\frac{\partial \bar{\phi}}{\partial \xi} = 0 \quad (27)$$

At $\xi = 1$, for $-\zeta_1 \le \zeta < 0$ and $1 \le \zeta \le \zeta_1 + 1$,

$$\frac{\partial \bar{\phi}}{\partial \xi} = 0 \quad (28)$$

At $\xi = 1$, for $0 \le \zeta \le 1$,

$$\bar{i}_2 = \frac{\partial \bar{\phi}}{\partial \xi} \quad (29)$$

At $\zeta = 0$ and $\zeta = \zeta_1 + 1$, for all ξ,

$$\bar{\phi} = 0 \quad (30)$$

The numerical discretization and the solution procedure of the bulk-diffusion model are given in Appendices A and C, respectively.

2.2. *Field model*

In this more rigorous approach, the electrolyte is not separated into two regions. The potential is coupled with the mass-transfer calculations. In addition to the depositing ion, the hydronium ion and the anion concentrations need to be included in the model. In all, five equations need to be solved simultaneously. These are the convective diffusion equations coupled with field effects for each species,

$$\begin{aligned} v_x \frac{\partial c_i}{\partial x} = {} & D_i\left(\frac{1}{y}\frac{\partial}{\partial y}\left[y\frac{\partial c_i}{\partial y}\right] + \frac{\partial}{\partial x}\left[\frac{\partial c_i}{\partial x}\right]\right) \\ & + z_i \mu_i F\left(c_i \frac{1}{y}\frac{\partial}{\partial y}\left[y\frac{\partial \phi}{\partial y}\right]\right. \\ & \left. + c_i \frac{\partial}{\partial x}\left[\frac{\partial \phi}{\partial x}\right] + \frac{\partial c_i}{\partial y}\frac{\partial \phi}{\partial y} + \frac{\partial \phi}{\partial x}\frac{\partial c_i}{\partial x}\right) \end{aligned} \quad (31)$$

with $i = 1$ for the depositing ion, $i = 2$ for the hydronium ion, $i = 3$ for the sulfate ion and $i = 4$ for the bisulfate ion and the electroneutrality equation,

$$\sum_{i=1}^{4} z_i c_i = 0 \quad (32)$$

In a recent copper deposition model by Goldbach et al. [8], they considered the acid copper sulfate solution to consist of three ions: Cu^{2+}, H^+ and HSO_4^- due to the high acid concentrations. Bortels et al. [10] have also considered the acid copper sulfate solution to consist of only three ions: Cu^{2+}, H^+, and SO_4^{2-} for a solution with a copper sulfate concentration of 0.01 M and a sulfuric acid concentration of 1.0 M. In general, the value of the ionization constant for the sulfuric acid is very large. Therefore, the sulfuric acid can be assumed to dissociate completely into the hydronium and bisulfate ions. However, the ionization constant, K_e, for the dissociation of the bisulfate ion into the hydronium and sulfate ions is related by the following equation:

$$K_e = \frac{c_{HSO_4^-}}{c_{H^+} c_{SO_4^{2-}}} \quad (33)$$

and is generally dependent on the sulfuric acid concentration. Different sulfuric acid concentrations in the copper plating solution are considered. Therefore, it is important to consider the copper plating solution to consist of four species: Cu^{2+}, H^+, SO_4^{2-}, and HSO_4^- in conjunction with the dissociation constant of the bisulfate ion.

The model assumes that the only heterogeneous reaction proceeding at the electrode is the metal deposition occurring at 100% current efficiency and neglects hydrolysis reactions occurring at the electrode during

metal ion depletion. This model does not consider secondary reactions, such as the hydrolysis of water and the evolution of hydrogen at more cathodic potentials. For the specific concentrations used, a discussion follows for those results when the model is no longer valid due to the occurrence of a secondary reaction.

The ionic mobility, μ_i, and the diffusion coefficient, D_i, for species i are related by the Nernst–Einstein relation:

$$\mu_i = \frac{D_i}{R_g T} \tag{34}$$

The boundary conditions are as follows:
At $x = -L_1$, for all y, $c_i = c_{i\infty}$,
with $i = 1, 2, 3$ and 4,

$$c_4 = \frac{-\sum_{j=1}^{3} z_j c_{j\infty}}{z_4} \quad \text{and} \quad \phi = 0 \tag{35}$$

At $x = L_1 + L_2$, for all y, $\dfrac{\partial c_i}{\partial x} = 0$, with $i = 1, 2, 3$ and 4,

$$\phi = 0 \tag{36}$$

At $y = R_0$, for $-L_1 \le x \le 0$,

$$z_i \mu_i F c_i \frac{\partial \phi}{\partial y} + D_i \frac{\partial c_i}{\partial y} = 0 \tag{37}$$

At $y = R_0$, for $L_1 \le x \le L_1 + L_2$,

$$z_i \mu_i F c_i \frac{\partial \phi}{\partial y} + D_i \frac{\partial c_i}{\partial y} = 0 \tag{38}$$

with $i = 1, 2, 3$ and 4.
At $y = 0$, for $-L_1 \le x \le L_1 + L_2$,

$$\frac{\partial c_i}{\partial y} = 0$$

with $y = 0$, and

$$\frac{\partial \phi}{\partial y} = 0 \tag{39}$$

At $y = R_0$, for $0 \le x \le L_2$,

$$z_1 \mu_1 F c_1 \frac{\partial \phi}{\partial y} + D_1 \frac{\partial c_1}{\partial y} = \frac{i}{nF}$$

with $i = 2, 3$ and 4, and

$$z_i \mu_i F c_i \frac{\partial \phi}{\partial y} + D_i \frac{\partial c_i}{\partial y} = 0 \tag{40}$$

In terms of the dimensionless variables, defined in Equations 16–18, and a dimensionless potential, $\bar{\phi}$,

$$\bar{\phi} = \frac{\phi F}{R_g T} \tag{41}$$

the governing equations are,

$$\begin{aligned} \bar{v}_x \frac{\partial \theta_i}{\partial \zeta} = {} & \frac{D_i}{D_1}\frac{1}{Pe}\left(2A_r \frac{1}{\xi}\frac{\partial}{\partial \xi}\left[\xi \frac{\partial \theta_i}{\partial \xi}\right] + \frac{1}{2A_r}\frac{\partial}{\partial \zeta}\left[\frac{\partial \theta_i}{\partial \zeta}\right]\right) \\ & + \frac{z_i}{Pe}\frac{D_i}{D_1}\left(2A_r \theta_i \frac{1}{\xi}\frac{\partial}{\partial \xi}\left[\xi \frac{\partial \bar{\phi}}{\partial \xi}\right] + \frac{\theta_i}{2A_r}\frac{\partial}{\partial \zeta}\left[\frac{\partial \bar{\phi}}{\partial \zeta}\right]\right) \\ & + \frac{z_i}{Pe}\frac{D_i}{D_1}\left(\frac{1}{2A_r}\frac{\partial \theta_i}{\partial \zeta}\frac{\partial \bar{\phi}}{\partial \zeta} + 2A_r \frac{\partial \theta_i}{\partial \xi}\frac{\partial \bar{\phi}}{\partial \xi}\right) \end{aligned} \tag{42}$$

with $i = 1, 2$ and 3, and

$$\sum_{i=1}^{4} z_i \theta_i = 0 \tag{43}$$

The boundary conditions are as follows:
At $\zeta = -\zeta_1$, for all ξ,

$$\theta_i = \frac{c_i}{c_{1\infty}}$$

with $i = 1, 2$ and 3, and

$$\theta_4 = \frac{-\sum_{j=1}^{3} z_j \theta_j}{z_4} \quad \text{and} \quad \bar{\phi} = 0 \tag{44}$$

At $\zeta = \zeta_1 + 1$, for all ξ,

$$\frac{\partial \theta_i}{\partial \zeta} = 0$$

with $i = 1, 2, 3$ and 4, and

$$\bar{\phi} = 0 \tag{45}$$

At $\xi = 1$, for $0 \le \zeta \le \zeta_1 + 1$,

$$z_i \theta_i \frac{\partial \bar{\phi}}{\partial \xi} + \frac{\partial \theta_i}{\partial \xi} = 0 \tag{46}$$

At $\xi = 1$, for $-\zeta_1 \le \zeta \le 0$,

$$z_i \theta_i \frac{\partial \bar{\phi}}{\partial \xi} + \frac{\partial \theta_i}{\partial \xi} = 0 \tag{47}$$

with $i = 1, 2, 3$ and 4.
At $\xi = 0$, for $-\zeta_1 \le \zeta \le \zeta_1 + 1$,

$$\frac{\partial \theta_i}{\partial \zeta} = 0$$

with $i = 1, 2, 3$ and 4, and

$$\frac{\partial \bar{\phi}}{\partial \xi} = 0 \tag{48}$$

At $\xi = 1$, for $0 \le \zeta \le 1$,

$$z_1 \theta_1 \frac{\partial \bar{\phi}}{\partial \xi} + \frac{\partial \theta_1}{\partial \xi} = \bar{i}_1$$

and

$$z_i\theta_i\frac{\partial\bar{\phi}}{\partial\xi}+\frac{\partial\theta_i}{\partial\xi}=0 \tag{49}$$

with $i = 2$, 3 and 4.

The numerical discretization and the solution procedure for the field model are given in Appendices B and C, respectively.

3. Results and discussion

3.1. *System with excess supporting electrolyte*

Table 1 shows a summary of the physical and kinetic parameters used in the simulation. α_a, α_c, i_0, n, and κ_∞ are typical parameters used by Pesco [5] in his through-hole model. D_1, D_2, D_3 and D_4 are the diffusion coefficients of the individual ions at infinite dilution [9]. The order of the reaction, γ, was calculated from Equation 5 by using parameters obtained from Pesco's paper [5]. The kinematic viscosity was assumed to have a value of $1.00 \times 10^{-2}\,cm^2\,s^{-1}$. Compared to the kinetic parameters used by Caban and Chapman [11], the statistical analysis of their experimental values for α_a, α_c, and i_0 yield slightly lower values.

The cathodic potentials and currents are taken to be positive values. A comparison between the bulk diffusion model and the field model is shown for a plating solution consisting of 0.01 M $CuSO_4$ and 2.0 M H_2SO_4. Following the work of Kessler and Alkire [12], a through-hole having an aspect ratio of 3.51 was chosen for this study, with a through-hole radius of 0.039 cm and a board thickness of 0.274 cm.

Using the geometric dimensions and chemical compositions as discussed above, polarization curves for both models at Peclet numbers of 100 and 100 000 are constructed in Figure 2. With an excess supporting electrolyte, good agreement is found between the two models. The surface concentration and the current distribution at different fractions of the limiting current are shown in Figure 3. The current density is highest at the entrance region of the through-hole and decreases in the direction of the flow. If these profiles were normalized with respect to the average current densities, less uniform profiles are observed at higher fractions of the limiting current. Similarly, the cupric ion concentration is higher at the entrance and decreases downstream. At the higher fractions of the limiting current, the cupric ion concentration is consumed faster and the entire profile is shifted downward. Again, the agreement between the two models is good.

Table 1. Physical and kinetic parameters

$\alpha_a = 0.75$
$\alpha_c = 0.25$
$\gamma = 0.75$
$n = 2$
$i_0 = 0.001\ A\ cm^{-2}$
$\kappa_\infty = 0.55\ (\Omega\ cm)^{-1}$
$D_1 = 0.55 \times 10^{-5}\,cm^2\,s^{-1}$
$D_2 = 9.312 \times 10^{-5}\,cm^2\,s^{-1}$
$D_3 = 1.065 \times 10^{-5}\,cm^2\,s^{-1}$
$D_4 = 1.33 \times 10^{-5}\,cm^2\,s^{-1}$
$v = 1.00 \times 10^{-2}\,cm^2\,s^{-1}$

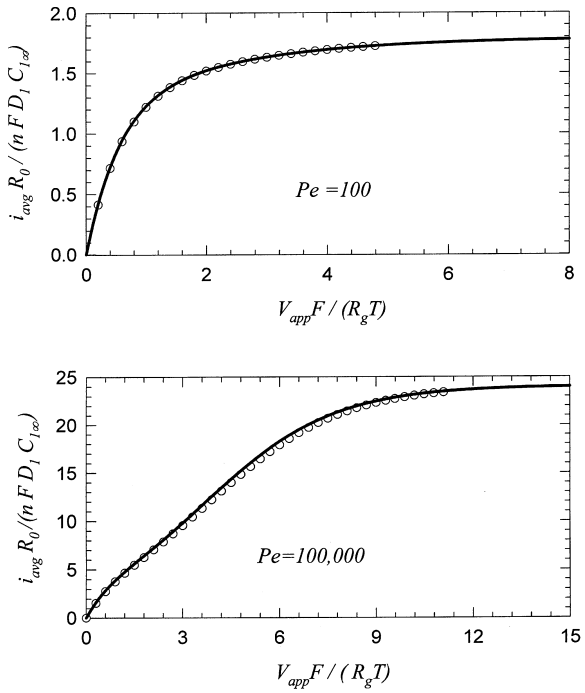

Fig. 2. Polarization curves. Key: (○) bulk diffusion model and (—) field model.

3.2. *System with low copper concentration*

The r value, proposed by Newman [9] , is an important parameter used to characterize the relative concentration of the reactant in comparison to the concentration of the supporting electrolyte.

$$r=\frac{C_{H^+}}{2C_{SO_4^{2-}}} \tag{50}$$

In a solution with an excess amount of a supporting electrolyte, the value of r approaches one. On the other extreme, $r = 0$ implies that the solution contains only a single salt. A solution consisting of 0.3 M $CuSO_4$ and 2.0 M H_2SO_4 is generally considered a lower copper plating bath with a r value of 0.87. With these plating conditions, numerical simulations are performed for both models and results are presented in Figures 4 and 5.

Figure 4 shows polarization curves for both models at a Peclet number of 100 000. Results show that a higher limiting current density is presented by the field model as compared to the bulk-diffusion model due to the enhancement of the flux by the effects of ionic migration. However, the magnitude of the average current density at a given applied potential for the field model is always

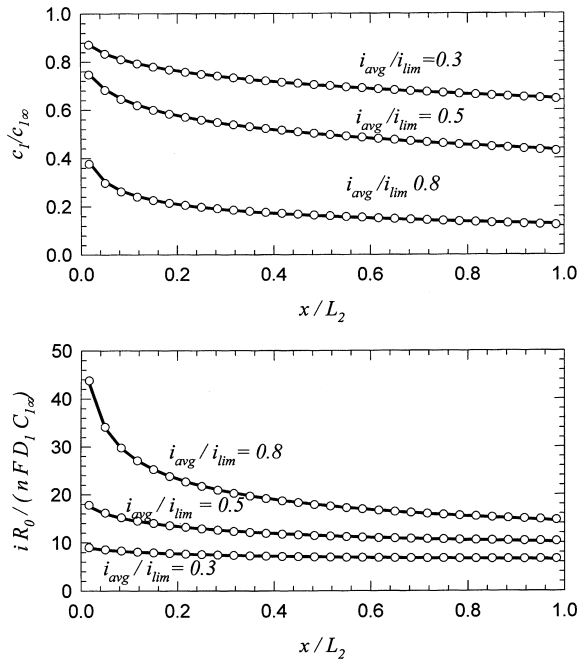

Fig. 3. Surface concentration profiles and current distributions at $Pe = 1 \times 10^5$. Key: (○) bulk diffusion model and (——) field model.

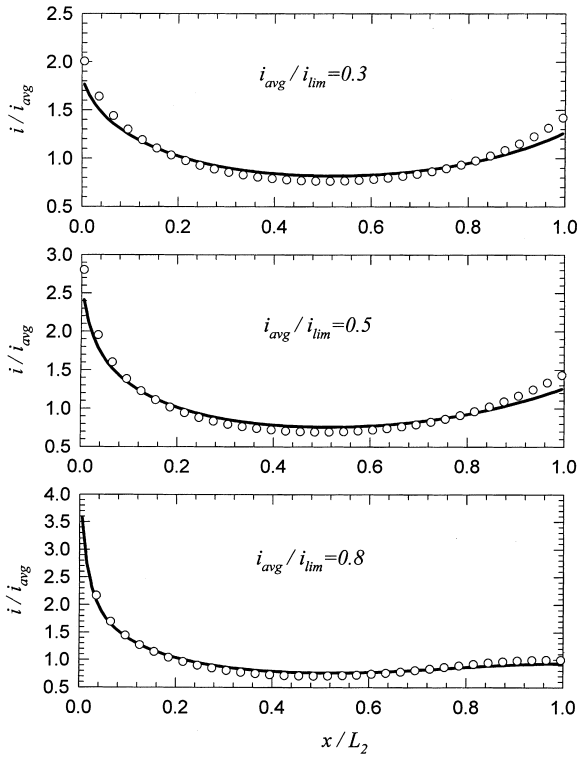

Fig. 5. Current distributions at $Pe = 1 \times 10^5$. Key: (○) bulk diffusion model and (——) field model.

higher than the bulk-diffusion. The general shape of the polarization curve also shows that a greater overpotential is required by the bulk-diffusion model to obtain 99% of its limiting current value. Based on the Nernst equation, it was estimated that hydrogen evolution starts to occur when the value of $V_{app}F/(R_gT)$ is approximately 14.6. Beyond this potential, both the deposition of metal and the evolution of hydrogen occur simultaneously on the electrode surface. For a solution with these concentrations, the model breaks down when the current exceeds approximately 50% of its limiting value.

Figure 5 shows a comparison of the normalized current distribution between the two models at the same fraction of the limiting current. At low fractions ($i_{avg}/i_{lim} = 0.3$) of the limiting current, the bulk diffusion models shows a slightly less uniform current distribution as compared to the field model due to a higher overpotential. The differences in the current distribution are most apparent at the leading and trailing edges of the working electrode. Based on the previous discussion, hydrogen starts to evolve when $i_{avg}/i_{lim} = 0.8$. The current distribution only considers the metal ion deposition and does account for any generation of hydrogen. In Figure 5 better agreement is found between the two models at higher fractions ($i_{avg}/i_{lim} = 0.8$) of the limiting current. Even for a copper plating solution with an r value as high as 0.87, this example shows differences in the current distribution between the two models. In both cases, secondary-like current distributions are shown at $i_{avg}/i_{lim} = 0.3$ where the mass transfer resistance is small. The current distribution is higher near both ends of the through-hole because of their proximity to the counter electrodes. At higher i_{avg}/i_{lim} values, the current distribution becomes less uniform. The current density becomes higher in the upstream region and lower in the downstream region, due to the effects of mass transfer.

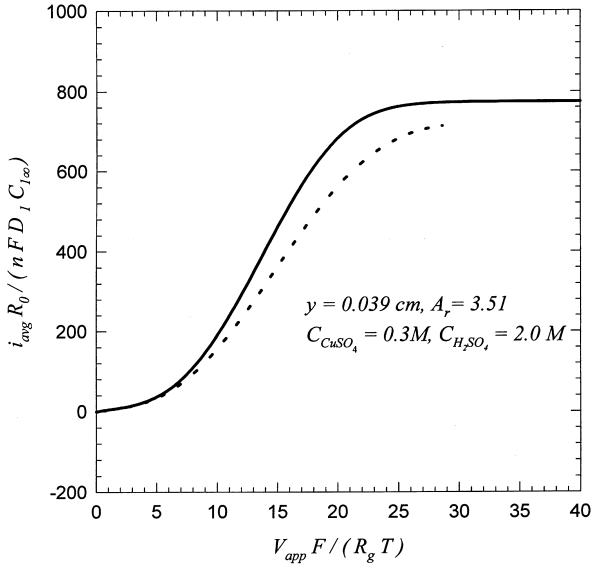

Fig. 4. Polarization curves at $Pe = 1 \times 10^5$. Key: (——) field model and (- - - -) bulk diffusion model.

3.3. *Solutions with different amounts of a supporting electrolyte*

Polarization curves for solutions containing the same copper sulfate concentration (C_{CuSO_4} = 0.3 M) but two different supporting electrolyte concentrations

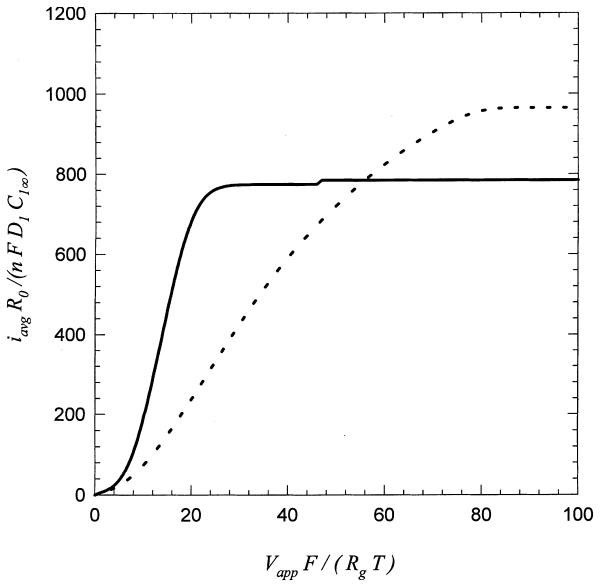

Fig. 6. Polarization curves at $Pe = 1 \times 10^5$. Key: (——) $r = 0.87$ and (- - - -) $r = 0.310$.

($c_{H_2SO_4} = 2.0$ M, $r = 0.87$ and $c_{H_2SO_4} = 0.135$ M, $r = 0.310$) are shown in Figure 6 for a Peclet number of 100 000. Polarization curves show that a higher applied potential is required to reach the limiting current for the solution containing less supporting electrolyte due to a lower electrolyte conductivity. On the other hand, the magnitude of the limiting current density is higher in the solution containing less supporting electrolyte because of the enhancement of ionic flux in a stronger electric field. The case for the concentration of a supporting electrolyte with a r value of 0.87 was already discussed in the previous Section. For the solution with a low concentration of a supporting electrolyte, it was estimated that hydrogen evolution starts to occur when the value of $V_{app}F/(R_gT)$ exceeds 15. These numerical values imply that the model begins to break down when the current exceeds approximately 40% of its limiting value.

Figure 7 shows a comparison of the current distributions at three different fractions of the limiting current for two concentrations of the supporting electrolyte. Similar to previous discussions, the current distribution results for $i_{avg}/i_{lim} = 0.3$ and 0.8 are unrealistic due to the onset of a secondary reaction. They are shown only to demonstrate the importance of the effect of ionic migration on the current distribution. A less uniform current distribution is observed in the solution containing less supporting electrolyte. Also, the appearance of a local maximum at $x/L = 0.95$ is shown in the solution containing less supporting electrolyte. This is due to a tradeoff between the decreasing ion concentration and the increasing field strength as the right of the hole is approached. At higher i_{avg}/i_{lim} values, the local maximum is displaced further upstream. The local maximum should disappear at $i_{avg}/i_{lim} = 1.0$ since the deposition is controlled solely by mass transfer.

Figure 8 shows the surface concentration profiles at various fractions of the limiting current for the two supporting electrolyte concentrations. Similar surface concentration profiles were shown by Hazelbeck and Talbot [6] for a r value of 0.87. Because of the assumption of a uniform bulk concentration by Hazelbeck and Talbot [6] at the leading edge of the electrode, all of their surface concentration values starts at the bulk value and decreases as it progresses along the positive axial direction. With our boundary conditions,

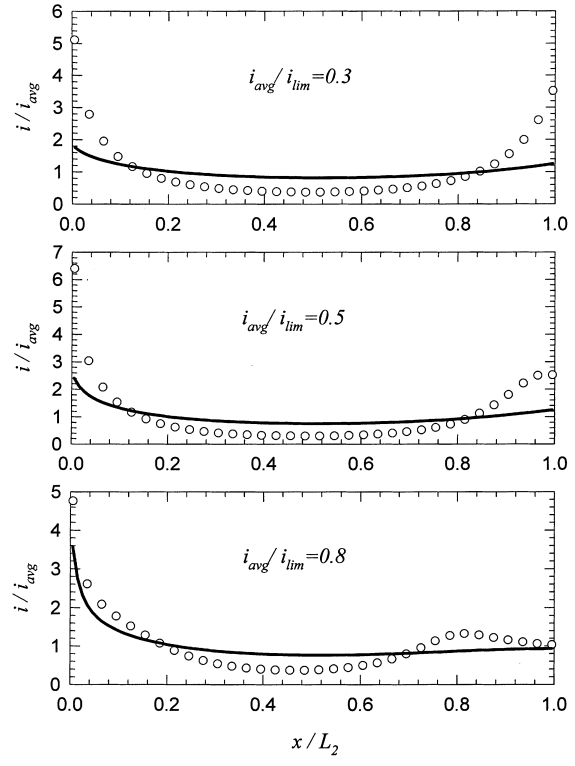

Fig. 7. Current distributions below the limiting current. Key: (——) $r = 0.874$ and (○) $r = 0.310$.

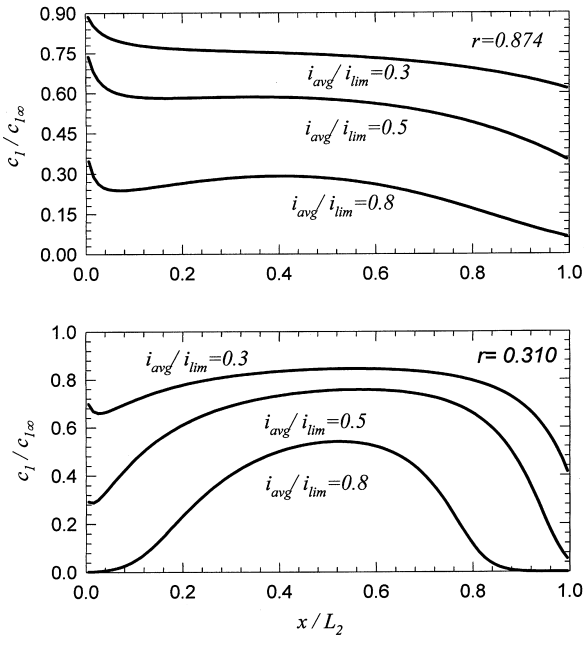

Fig. 8. Surface concentration profiles at $Pe = 1 \times 10^5$.

results show that the value of the dimensionless surface concentration is highest in the upstream region but not equal to one at $x/L_2 = 0$ for a r value of 0.87. At low fractions ($i_{avg}/i_{lim} = 0.3$ and 0.5) of the limiting current, the trend is that the surface concentration profile decreases in the downstream region due to the depletion of cupric ions at the electrode surface as the electrolyte travels from the left to the right. However, at high fractions ($i_{avg}/i_{lim} = 0.8$) of the limiting current, the surface concentration profile decreases initially, forms a local maximum at $x/L_2 = 0.5$, and then decreases downstream. At a sulfuric acid concentration of 0.135 M, field effects become important. The more reactive portions of the through-hole are regions more accessible to the counter electrodes. At higher i_{avg}/i_{lim} values, the appearance of a global maximum in the surface concentration within the through-hole is observed.

4. Conclusions

Results are shown for a through-hole geometry with an aspect ratio of 3.51 and a radius of 0.039 cm. For copper plating solutions with an r value of 0.87 ($c_{CuSO_4} = 0.3$ M), numerical simulation shows that a larger overpotential is required by the bulk-diffusion model to obtain the same average current density as compared to the field model. For the same i_{avg}/i_{lim} value for both models, a more uniform current distribution is predicted by the field model. The results show that the field model should be used to estimate the current distribution in through-hole electrodeposition even for supporting electrolyte concentrations with r values as high as 0.87. Generally, secondary-like current distributions are obtained for $i_{avg}/i_{lim} \leq 0.3$ while mass-transfer effects dominate at $i_{avg}/i_{lim} \geq 0.8$. Both kinetic and mass transfer effects are important at intermediate current levels. Results show the current profiles from the bulk-diffusion model converge to the results from the field model in the presence of a large amount of a supporting electrolyte.

The current formulation of the bulk diffusion model considers the effect of back diffusion since the boundary condition of the cupric ion is set equal to the bulk value far upstream away from the entrance of the electrode. With this type of boundary condition, the bulk diffusion model is generally valid for all Peclet numbers in the presence of an excess amount of a supporting electrolyte. However, when the amount of a supporting electrolyte is not in excess ($r \leq 0.95$), the more rigorous field model should be used to accurately predict the current distribution due to the effect of ionic migration.

References

1. A.M. Pesco and H.Y. Cheh, *J. Electrochem. Soc.* **136** (1989) 399.
2. R. Alkire and A.A. Mirarefi, *J. Electrochem. Soc.* **124** (1977) 1043.
3. J.E. Chern and H.Y. Cheh, *J. Electrochem. Soc.* **143** (1996) 3139.
4. J.E. Chern and H.Y. Cheh, *J. Electrochem. Soc.* **143** (1996) 3144.
5. A.M. Pesco and H.Y. Cheh, *J. Electrochem. Soc.* **136** (1989) 408.
6. D.A. Hazlebeck and J.B. Talbot, *J. Electrochem. Soc.* **138** (1991) 1985.
7. D.A. Dudek and P.S. Fedkiw, *J. Electroanal. Chem.* **474** (1999) 31.
8. S. Goldbach, B. Bossche, T. Daenen, J. Deconinck and F. Lapicque, *J. Appl. Electrochem.* **30** (2000) 1.
9. J.S. Newman, 'Electrochemical Systems', 2nd edn (Prentice Hall, New Jersey, 1991).
10. V.D. Bossche, L. Bortels, J. Deconinck, S. Vandeputte and A. Hubin, *J. Electroanal. Chem.* **397** (1995) 35.
11. R. Caban and T.W. Chapman, *J. Electrochem. Soc.* **124** (1977) 1371.
12. T. Kessler and R. Alkire, *J. Electrochem. Soc.* **123** (1976) 990.
13. V. Patankar, 'Numerical Heat Transfer and Fluid Flow' (Hemisphere Publishing, New York, 1996).
14. J. Newman, *Int. J. Heat Mass Transf.* **10** (1967) 983.
15. W. Engelmaier and T. Alkire, *J. Electrochem. Soc.* **125** (1978) 36.
16. R. Haak, C. Ogden and D. Tench, *J. Appl. Electrochem.* **11** (1981) 771.
17. T. Kessler and R. Alkire, *Plati. Surf. Finish.* **63** (1976) 22.
18. T.W. Lee, PhD dissertation, Columbia University (1996).
19. T. Sullivan and S. Middleman, *J. Electrochem. Soc.* **132** (1985) 1050.
20. T. Sullivan and S. Middleman, *J. Electrochem. Soc.* **133** (1986) 492.
21. D.R. Turner and G.R. Johnson, *J. Electrochem. Soc.* **109** (1962) 798.
22. E.K. Yung, L.T. Romankiw and R.C. Alkire, *J. Electrochem. Soc.* **136** (1989) 206.

Appendix A: Numerical discretization of the bulk diffusion model

The following indices were used for the 2D control volume formulation of the mass-transfer equation: i for the axial direction and j for the radial direction.

We began by setting up a material balance on the control volume, shown in Figure 9, for the convective diffusion equation,

$$J_t 2\pi\xi_t\Delta\zeta - J_b 2\pi\xi_b\Delta\zeta + J_r\pi(\xi_t^2 - \xi_b^2) - J_l\pi(\xi_t^2 - \xi_b^2) = 0 \quad \text{(A1)}$$

where J_t, J_b, J_r and J_l are the dimensionless integrated total fluxes through the top, bottom, right and left face of control volume, respectively. That is,

$$J_t = D_t(\theta_{i,j} - \theta_{i,j+1}) \quad \text{(A2)}$$

$$J_b = D_b(\theta_{i,j-1} - \theta_{i,j}) \quad \text{(A3)}$$

$$J_r = F_r\theta_{i,j} + a_r(\theta_{i,j} - \theta_{i+1,j}) \quad \text{(A4)}$$

$$J_l = F_l\theta_{i,j} + a_l(\theta_{i-1,j} - \theta_{i,j}) \quad \text{(A5)}$$

F_r and F_l were the dimensionless local convective fluxes acting on the faces of the control volume,

$$\delta\xi_t = \frac{\delta_y(i,j+1) + \delta_y(i,j)}{2} \quad \text{(A6)}$$

$$\delta\xi_b = \frac{\delta_y(i,j) + \delta_y(i,j-1)}{2} \quad \text{(A7)}$$

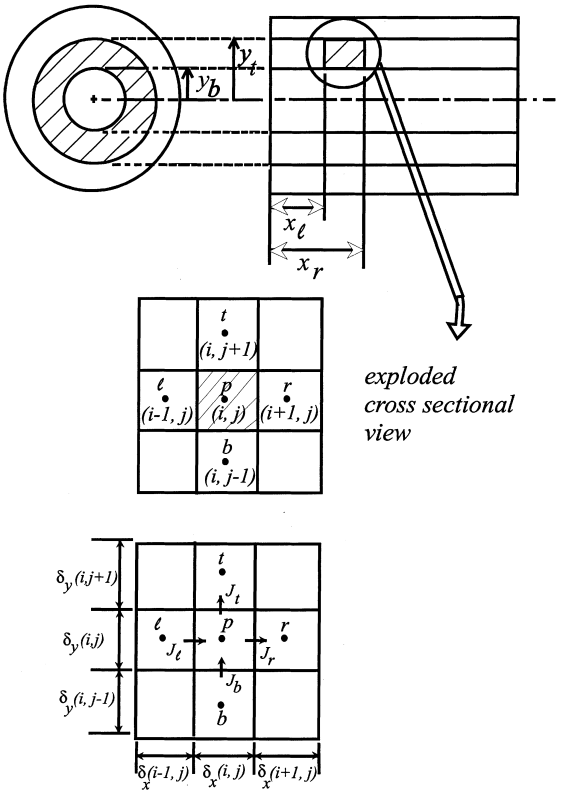

Fig. 9. Control volume formulation for cylindrical geometry.

$$\delta\zeta_r = \frac{\delta_x(i+1,j) + \delta_x(i,j)}{2} \tag{A8}$$

$$\delta\zeta_l = \frac{\delta_x(i,j) + \delta_x(i-1,j)}{2} \tag{A9}$$

$$D_t = \frac{1}{Pe}\frac{\xi_t}{\delta\xi_t}\delta\zeta_i \tag{A10}$$

$$D_b = \frac{1}{Pe}\frac{\xi_b}{\delta\xi_b}\delta\zeta_i \tag{A11}$$

$$F_r = \frac{\bar{v}_{xr}}{2A_r}\left(\frac{\xi_t + \xi_b}{2}\right)\delta\xi_j \tag{A12a}$$

$$D_r = \frac{1}{Pe}\frac{1}{(2A_r)^2}\frac{1}{\delta_r}\frac{(\xi_t + \xi_b)}{2}\delta\xi_j \tag{A12b}$$

$$F_l = \frac{\bar{v}_{xl}}{2A_r}\left(\frac{\xi_n + \xi_s}{2}\right)\delta\xi_j \tag{A13a}$$

$$D_l = \frac{1}{Pe}\frac{1}{(2A_r)^2}\frac{1}{\delta\zeta_l}\frac{(\xi_t + \xi_b)}{2}\delta\xi_j \tag{A13b}$$

where D_t, D_b, D_r and D_l were the dimensionless local diffusive fluxes through the face of the control volume.

$$a_r = D_r A(|P_r|) + \|-F_r, 0\| \tag{A14}$$

$$a_l = D_l A(|P_l|) + \|F_l, 0\| \tag{A15}$$

P_r and P_l were defined as the local Peclet number on the right and left faces of the control volume, respectively. That is,

$$A(|P_r|) = \left\|0, (1 - 0.1|P_r|)^5\right\| \tag{A16}$$

$$A(|P_l|) = \left\|0, (1 - 0.1|P_l|)^5\right\| \tag{A17}$$

where

$$P_r = \frac{F_r}{D_r} \quad \text{and} \quad P_l = \frac{F_l}{D_l} \tag{A18}$$

A power law scheme [13] valid at both the low and high Peclet number range was adopted in the present work.

In the bulk electrolyte, a material balance on the representative control volume was set up and shown in Figure 9, for the Laplace equation. That is,

$$J_t 2\pi\xi_t\Delta\zeta - J_b 2\pi\xi_b\Delta\zeta + J_r\pi(\xi_t^2 - \xi_b^2) - J_l\pi(\xi_t^2 - \xi_b^2) = 0 \tag{A19}$$

$$J_t = \frac{\bar{\phi}_{i,j} - \bar{\phi}_{i,j+1}}{\delta\xi_t} \tag{A20}$$

$$J_b = \frac{\bar{\phi}_{i,j-1} - \bar{\phi}_{i,j}}{\delta\xi_b} \tag{A21}$$

$$J_r = \frac{\bar{\phi}_{i,j} - \bar{\phi}_{i+1,j}}{\delta\zeta_r} \tag{A22}$$

$$J_l = \frac{\bar{\phi}_{i-1,j} - \bar{\phi}_{i,j}}{\delta\zeta_l} \tag{A23}$$

where J_t, J_b, J_r and J_l referred to the dimensionless integrated total fluxes through the top, bottom, right and left control volume faces, respectively.

The numerical solution of these simultaneous difference equations was obtained by using the subroutine BANDJ [9].

Appendix B: Numerical discretization of the field model

Due to the highly nonlinear nature of the partial differential equations, the dependent variables were linearized around a guess value.

$$\theta_i(\zeta,\xi) = \theta_i^0(\zeta,\xi) + \Delta\theta_i(\zeta,\xi) \tag{B1}$$

$$\bar{\phi}(\zeta,\xi) = \bar{\phi}^0(\zeta,\xi) + \Delta\bar{\phi}(\zeta,\xi) \tag{B2}$$

where $\theta_i^0(\zeta,\xi)$ and $\bar{\phi}^0(\zeta,\xi)$ were the guess values, while $\Delta\theta_i(\zeta,\xi)$ and $\Delta\bar{\phi}(\zeta,\xi)$ were defined as the difference

between the actual value and the guess value, and $\theta_i(\zeta,\xi)$ and $\bar{\phi}(\zeta,\xi)$ were the actual values.

A material balance on the representative control volume for a species is given by

$$J_t 2\pi\xi_t\Delta\zeta - J_b 2\pi\xi_b\Delta\zeta + J_r\pi({\xi_t}^2 - {\xi_b}^2) - J_l\pi(\xi_t^2 - \xi_b^2) = 0 \tag{B3}$$

where J_t, J_b, J_r and J_l referred to the dimensionless integrated total fluxes through the top, bottom, right and left control volume faces, respectively. That is,

$$J_t = D_t(\theta_{i,j} - \theta_{i,j+1}) - z_i\theta_t^0(\bar{\phi}_{i,j+1} - \bar{\phi}_{i,j})D_t - z_i(D_t\delta\xi_t)\frac{\partial\bar{\phi}^0}{\partial\xi}\bigg|_t\theta_t + z_i(D_t\delta\xi_t)\frac{\partial\bar{\phi}^0}{\partial\xi}\bigg|_t\theta_t^0 \tag{B4}$$

$$J_b = D_b(\theta_{i,j-1} - \theta_{i,j}) - z_i\theta_b^0(\bar{\phi}_{i,j} - \bar{\phi}_{i,j-1})D_b - z_i(D_b\delta\xi_b)\frac{\partial\bar{\phi}^0}{\partial\xi}\bigg|_b\theta_b + z_i(D_b\delta\xi_b)\frac{\partial\bar{\phi}^0}{\partial\xi}\bigg|_b\theta_b^0 \tag{B5}$$

$$J_r = F_r\theta_{i,j} + a_r(\theta_{i,j} - \theta_{i+1,j}) - z_i\theta_r^0(\phi_{i+1,j} - \bar{\phi}_{i,j})D_r - \frac{\partial\bar{\phi}^0}{\partial\zeta}\bigg|_r\theta_r^0(\delta\zeta_r D_r)z_i - z_i(\delta\zeta_r D_r)\theta_r\frac{\partial\bar{\phi}^0}{\partial\zeta}\bigg|_r \tag{B6}$$

$$J_l = F_l\theta_{i,j} + a_l(\theta_{i-1,j} - \theta_{i,j}) - z_i\theta_l^0(\bar{\phi}_{i,j} - \phi_{i-1,j})D_l - \frac{\partial\bar{\phi}^0}{\partial\zeta}\bigg|_l\theta_l^0(\delta\zeta_l D_l)z_i + z_i(\delta\zeta_l D_l)\theta_l\frac{\partial\phi^0}{\partial\zeta}\bigg|_l \tag{B7}$$

F_r and F_l were the dimensionless local convective fluxes through the faces of the control volume.

$$\delta\xi_t = \frac{\delta_y(i,j+1) + \delta_y(i,j)}{2} \tag{B8}$$

$$\delta\xi_b = \frac{\delta_y(i,j) + \delta_y(i,j-1)}{2} \tag{B9}$$

$$\delta\zeta_r = \frac{\delta_x(i+1,j) + \delta_x(i,j)}{2} \tag{B10}$$

$$\delta\zeta_l = \frac{\delta_x(i,j) + \delta_x(i-1,j)}{2} \tag{B11}$$

$$D_t = \frac{1}{P_r}\frac{\xi_t}{\delta\xi_t}\delta\zeta_i \tag{B12}$$

$$D_b = \frac{1}{P_r}\frac{\xi_b}{\delta\xi_b}\delta\zeta_i \tag{B13}$$

$$F_r = \frac{\bar{v}_{xr}}{2A_r}\left(\frac{\xi_t + \xi_b}{2}\right)\delta\xi_j \tag{B14a}$$

$$D_r = \frac{1}{Pe}\frac{1}{(2A_r)^2}\frac{1}{\delta\zeta_r}\frac{(\xi_t + \xi_b)}{2}\delta\xi_j \tag{B14b}$$

$$F_l = \frac{\bar{v}_{xl}}{2A_r}\left(\frac{\xi_t + \xi_b}{2}\right)\delta\xi_j \tag{B15a}$$

$$D_l = \frac{1}{Pe}\frac{1}{(2A_r)^2}\frac{1}{\delta\zeta_l}\frac{(\xi_t + \xi_b)}{2}\delta\xi_j \tag{B15b}$$

D_t, D_b, D_r and D_l were the dimensionless local diffusive fluxes through the faces of the control volume.

$$a_r = D_r A(|P_r|) + \|-F_r, 0\| \tag{B16}$$

$$a_l = D_l A(|P_l|) + \|F_l, 0\| \tag{B17}$$

P_r and P_l were defined as the local Peclet number on the east and west faces of the control volume, respectively.

$$A(|P_r|) = \left\|0, (1 - 0.1|P_r|)^5\right\| \tag{B18}$$

$$A(|P_l|) = \left\|0, (1 - 0.1|P_l|)^5\right\| \tag{B19}$$

The power law scheme [13] was once again adopted in the present work.

$$P_r = \frac{F_r}{D_r} \quad \text{and} \quad P_l = \frac{F_l}{D_l} \tag{B20}$$

$$\theta_t = \frac{\theta_{i,j+1}\delta\xi_{j+1} + \theta_{i,j}\delta\xi_j}{\delta\xi_{j+1} + \delta\xi_j} \tag{B21}$$

$$\theta_b = \frac{\theta_{i,j}\delta\xi_j + \theta_{i,j+1}\delta\xi_{j-1}}{\delta\xi_j + \delta\xi_{j-1}} \tag{B22}$$

$$\theta_r = \frac{\theta_{i+1,j}\delta\zeta_{i+1} + \theta_{i,j}\delta\zeta_i}{\delta\zeta_{i+1} + \delta\zeta_i} \tag{B23}$$

$$\theta_l = \frac{\theta_{i,j}\delta\zeta_i + \theta_{i-1,j}\delta\zeta_{i-1}}{\delta\zeta_i + \delta\zeta_{i-1}} \tag{B24}$$

$$\frac{\partial\bar{\phi}^0}{\partial\xi}\bigg|_b = \frac{\bar{\phi}_{i,j}^0 - \bar{\phi}_{i,j-1}^0}{\delta\xi_b} \tag{B25}$$

$$\frac{\partial\bar{\phi}^0}{\partial\xi}\bigg|_t = \frac{\bar{\phi}_{i,j+1}^0 - \bar{\phi}_{i,j}^0}{\delta\xi_t} \tag{B26}$$

$$\frac{\partial\bar{\phi}^0}{\partial\zeta}\bigg|_r = \frac{\bar{\phi}_{i+1,j}^0 - \bar{\phi}_{i,j}^0}{\delta\zeta_r} \tag{B27}$$

$$\frac{\partial\bar{\phi}^0}{\partial\zeta}\bigg|_l = \frac{\bar{\phi}_{i,j}^0 - \bar{\phi}_{i-1,j}^0}{\delta\zeta_l} \tag{B28}$$

The numerical solution of these simultaneous difference equations was obtained by using the subroutine BANDJ [9].

Appendix C: Solution procedure

C1. *Bulk-diffusion model*

Equations 20–30 subject to appropriate boundary conditions, were solved as follows:

1. Input the reactant bulk concentration, $c_{1\infty}$, and the applied potential, V_{app}.
2. Initially, the concentration and the potential everywhere in the domain were set equal to the bulk concentration and the applied potential, respectively.
3. The concentration was updated by solving the convective diffusion equation from the previously known values of the concentration and the potential.
4. Using the new concentration, the current distribution, i_{CD}, was calculated.
5. The potential was updated by solving the Laplace equation from the previous potential and the updated concentration.
6. Using the new potential, the current distribution, i_{LP}, was calculated
7. If $|i_{CD}(x) - i_{LP}(x)|$ was greater than 10^{-6}, steps 3–7 were repeated.
8. If $|i_{CD}(x) - i_{LP}(x)|$ was less than 10^{-6}, the solution was obtained.

C2. *Field model*

Equations 42–49 with the appropriate boundary conditions were solved as follows:

1. Input the charge and the bulk concentrations for each of the individual species (z_1, z_2, z_3, z_4, $c_{1\infty}$, $c_{2\infty}$, $c_{3\infty}$, $c_{4\infty}$).
2. Input the applied potential, V_{app}.
3. Initially, the concentration and the potential everywhere in the domain were set equal to the bulk concentration and the applied potential, respectively.
4. The concentration and the potential were updated by solving the four field equations plus the electroneutrality condition using the previously known values of the concentration and the potential.
5. Let

$$\left|c_1^N(x,r) - c_1^P(x,r)\right| = err1$$

$$\left|c_2^N(x,r) - c_2^P(x,r)\right| = err2$$

$$\left|c_3^N(x,r) - c_3^P(x,r)\right| = err3$$

$$\left|c_4^N(x,r) - c_4^P(x,r)\right| = err4$$

$$\left|\phi^N(x,r) - \phi^P(x,r)\right| = err5$$

The superscript N referred to the updated values while the superscript P referred to the values from the previous iteration. Also,

$$err = \mathrm{Max}|err1, err2, err3, err4, err5|$$

If err was greater than 10^{-6}, step 4 was repeated.